LBL-34006
UC-411
Preprint

Lawrence Berkeley Laboratory
UNIVERSITY OF CALIFORNIA

CHEMICAL SCIENCES DIVISION

Submitted to Physical Review A

Alignment of Magnetic Substates in Double Electron Capture Collisions

M.H. Prior, R.A. Holt, D. Schneider,
K.L. Randall, and R. Hutton

April 1993

Prepared for the U.S. Department of Energy under Contract Number DE-AC03-76SF00098

DISCLAIMER

LBL-34006

Alignment of Magnetic Substates in Double Electron Capture Collisions

M. H. Prior
Chemical Sciences Division, Lawrence Berkeley Laboratory,
University of California, Berkeley, California 94720

R.A. Holt*
Dept. of Physics, U. Western Ontario,
London, Ontario, Canada N6A 3K7

D. Schneider
V-Division, Lawrence Livermore National Laboratory,
P. O. Box 808, Livermore, California 94550

K.L. Randall**
Dept. of Chemistry, U. Toronto,
Toronto, Canada M5S 1A1

R. Hutton*
Dept. of Physics, Univ. of Lund, S-223 62 Lund, Sweden

This work was performed under the auspices of the U.S. Department of Energy by Lawrence Livermore National Laboratory under Contract No. W-7405-Eng-48, and by Lawrence Berkeley Laboratory with support from the Director, Office of Energy Research, Office of Basic Energy Sciences, Chemical Sciences Division, of the U.S. Department of Energy under Contract No. DE-AC03-76SF00098.

ABSTRACT

We have determined the magnetic substate alignment produced in double electron capture by the H-like projectiles C^{5+} and B^{4+} from He atoms by measuring the anisotropy of the Auger electron emission from the doubly excited 1s2l2l' ^{2}L projectile states formed in the collision. This work adds recent results to, and expands upon, our previous short communication on the C^{5+}, He system [Phys. Rev. **A43**, 607 (1991)] These are the first determinations of M_L substate populations produced by a multiple electron capture collision and they challenge theory at the nearly the finest quantum state detail. We observe large differences between the results for B^{4+} and C^{5+} over the velocity range 0.25-0.50 au for the substate and total 1s2l2l' ^{2}L relative cross-sections. Substantial population of $M_L>0$ states shows the importance of rotational coupling in these slow collisions. The large anisotropies observed demonstrate that substantial errors can result from inferring "cross-sections" from single angle measurements and the assumption of isotropic electron emission.

PACS numbers: 34.70.+e, 32.80.Dz

I. Introduction

Multiple electron capture in slow ion atom collisions produces multiply excited ionic states which may reveal their quantum properties through analysis of subsequent photon or Auger electron emission. In contrast to studies of the allowed photon emission, which are limited to the dipole term (see e.g. [1]), the Auger spectrum can yield information on all orders of multipolarity of the excited electronic wavefunction, since probabilities are often high for emission of electrons carrying away any amount of angular momentum. In the desirable case where the final ion state has zero total orbital angular momentum, i.e. an S state, the angular variation of the Auger electron emission, with respect to the projectile beam direction, carries complete information on the substate alignment created in the capture process [2]. In this work we report studies of such collisions where the projectile carries one electron and the target is a helium atom. That is the collision system:

$$A^{(Z-1)+}(1s) + He(1s^2\ ^1S_0) \rightarrow A^{(Z-3)+}(1s2l2l'\ ^2L) + He^{++}$$

analyzed by study of the angular variation of the Auger electron emission

$$A^{(Z-3)+}(1s2l2l'\ ^2L) \rightarrow A^{(Z-2)+}(1s^2\ ^1S_0) + e^-(\epsilon L)$$

for the case where $A^{(Z-1)+}=B^{4+}$, and C^{5+}. The work's major application is as a detailed test of two-electron capture theory in the low energy ($v<1$ au) regime. However, the demonstration of large energy-dependent anisotropies has impact upon total cross-section measurements and points out the possibility of probing fine scale properties of some long-lived doubly-excited states via induced perturbation of the collision-produced alignment. The majority of our results from study of the C^{5+},He system have appeared

in brief form [3]. They are included here, together with new results for this system, for completeness and for comparison with the new B^{4+} + He results.

II. Experimental Method

These experiments were made at the LBL/LLNL (Lawrence Berkeley Lab./Lawrence Livermore National Lab.) atomic physics facility located at the LBL 88-inch cyclotron. Fig. 1 shows a view of the portion of the facility which draws ions from the original LBL ECR (Electron Cyclotron Resonance) ion source. The B^{4+} ions were produced by feeding B_2O_3 vapor from a resistance heated Ta oven ($\approx$ 1500°C) radially into the ECR plasma chamber which was operating with a hydrogen support plasma. The C^{5+} ions were made from CO gas fed directly into the plasma chamber, which was operated with a He support plasma. Beams were momentum analyzed by the 90° magnet, directed and focused by the 70° magnet, x/y steering plates, and einzel lens into the chamber containing a rotatable electron spectrometer and gas jet (upper beam line in Fig. 1). This apparatus is shown in Fig. 2. The spectrometer is a 45° parallel plate analyzer which rests on a turntable with a resistance readout of the table position; the entire assembly is inside a double-walled mu-metal magnetic shield. The spectrometer design allows coverage of angles between 20° and 160° (0° is along the beam direction). The ion beams were collimated to 3x3 mm^2 with $\approx$5 mrad divergence by passage through 4-jaw collimators separated by 1.2m. At 10 x q keV, typical charge analyzed currents (at the exit slit of the 90° magnet) were about 3.0 μA for both ions; the resulting transmitted current to the Faraday cup at the exit of the spectrometer chamber was about 5.0 nA.

The beams intersected a He gas jet with three-axis adjustment to allow alignment with the turntable axis and optimum positioning of the jet assembly above the beam. To improve the resolution of the spectrometer, the electrons (at about 250 eV for the C^{5+} and 150 eV for B^{4+} projectiles) were decelerated before reaching the entrance slit to energies between 40 and 60 eV. At the exit of the spectrometer, the electrons were accelerated into a channel electron multiplier (CEM). Pulses from the CEM, after amplification and discrimination, passed into a multichannel scaling (MCS) system based upon a microcomputer. The MCS system scanned the voltages on the spectrometer to cover selected laboratory electron energy ranges; the dwell time in each channel was that required to reach a preset charge into the Faraday cup as determined by an integrating electrometer.

III. Spectra and Alignment Measurements

Figures 3 and 4 show spectra from both ions taken at a laboratory angle of 160°. The prominent lines are from $1s(2l2l')\ ^2L$ states where the active electrons, originating in the spin singlet state of the He ground state, are captured into one of the $2l2l'$ singlet states, yielding the final states: $1s2s^2\ ^2S$, $1s[2s2p\ ^1P]^2P$, $1s2p^2\ ^2D$, and ^2S. Henceforth we use the abreviations: $S_a \equiv 1s2s^2\ ^2S$, $P_a \equiv 1s[2s2p\ ^3P]^2P$, $P_b \equiv 1s[2s2p\ ^1P]^2P$, $D \equiv 1s2p^2\ ^2D$, and $S_b \equiv 1s2p^2\ ^2S$. Tables 1 and 2 summarise properties of the states arising from the $1s2l2l'$ configurations in B^{2+} and C^{3+} respectively. Since the collision is fast compared to spin-orbit coupling times and is dominated by the Coulomb interactions, it is expected that the captured electrons will remain in a singlet state. Although labeled with "valence" configurations $[2s2p\ ^1P]$ or $[2s2p\ ^3P]$, the two ^2P states each contain some

opposite spin character and therefore population of $1s[2s2p\ ^3P]\ ^2P$ is possible when capturing 2 electrons from a pure spin singlet state. Some intensity is seen in Figs. 3 and 4 from decay of the $1s2s2p\ ^4P$ state. This state is not a pure quartet since it contains components of singlet valence character due to mixing by the fine-structure interaction with, most significantly, the $1s[2s2p\ ^1P]^2P$ state. It is, however, the lowest member of the "quartet" system; none of these states, to the extent that they are pure quartets, may Auger decay via the Coulomb operator, but rather radiatively decay, perhaps in several steps, to $1s2s2p\ ^4P$. Thus one could expect to see some intensity from $1s2s2p\ ^4P$ because, 1) it is weakly produced directly via its valence singlet character and 2) it collects virtually all the population of higher lying quartet states which radiatively feed it. Ultimately $1s2s2p\ ^4P$ does Auger decay via the Coulomb coupling to its ^2L components and by the coupling to the continuum of its major quartet component by the spin-spin part of the Breit interaction. The reader is referred to the extensive series of theoretical papers on these states [4-15].

Another mechanism for populating states with triplet valence spin states is two separate single capture collisions, either with the He gas or in combination with one capture from the residual gas in the beam transport line to the apparatus. Careful studies were made of the variation of the intensity of the principle Auger lines with He jet density, monitored by measuring the chamber ambient He pressure. Data were collected well within the single collision regime where the line intensities varied linearly with the density.

The alignment created in the P_b and D states of each ion was determined by normalizing the area of the peaks from these states to the area of one of the peaks from

the $S_{a,b}$ states (S_a for B^{2+} and S_b for C^{3+}). This was done for spectra taken at nine angles ranging from 20° to 160° in the laboratory. Normalizing to the isotropic S states obviates the need to correct for changing overlap of the viewing angle of the spectrometer with the beam-jet intersection, gas jet density, transmission of the spectrometer, CEM detector gain, or electronic thresholds, etc. This normalization was accomplished by fitting an appropriate line shape to each peak in the spectra and then calculating the areas under the line shapes for the P_b, D and chosen S peaks. For the C^{5+} projectile data, a gaussian line shape of constant width for all lines fit the data well. For the B^{4+} data, an asymmetric "gaussian" shape was used. As seen in Fig. 3, the boron spectrum shows small but noticeable broadening on the low energy side which may reflect post-collisional effects (see the following section).

The normalized intensity, $I_L(\theta) \equiv$(ratio of peak areas), at angle θ from a state with angular momentum L is given by,

$$I_L(\theta) = \frac{\sigma_L}{\sigma_S} W_L(\theta), \tag{III.1}$$

with,

$$W_L(\theta) = 1 + \sum_{k=1}^{L} D_{2k} A_{2k} P_{2k}(\cos\theta). \tag{III.2}$$

where σ_L and σ_S are cross sections for producing the states, the $P_{2k}(\cos\theta)$ are Legendre polynomials, the A_{2k} are alignment coefficients to be determined and the D_{2k} are factors near unity, which correct for de-alignment caused by the incomplete fine-structure coupling of $\vec{L}$ and $\vec{S}$ during the period before the Auger decay [16]. This treatment is appropriate for cases where post-collision interaction effects which can alter the angular distribution are insignificant (see following section).

Figs. 5 and 6 show our anisotropy data and the least-squares best fit of Eq. (III.2) made by adjusting the parameters $A_{2k}^{eff} \equiv D_{2k}A_{2k}$ and σ_L/σ_S. Table 3 contains the A_{2k} and σ_L/σ_S values extracted from the fits using values for the D_{2k} calculated following [16] from parameters contained in Tables 1 and 2. Also included in Table 3 are the magnetic substate fractions inferred from the A_{2k} (see Section V).

IV. Post Collision Interaction Effects

Perturbation of Auger line shapes, positions and angular distributions caused by the proximity of the target product ion to the excited projectile when the electron emission occurs are termed post collision interaction (PCI) effects. There are a number of these which include focusing of electron trajectories and shift of the electron energy by the Coulomb potential of the target product ion. The electric field of the target ion can also mix opposite parity excited states producing a forward/backward asymmetry in the angular distribution (since the field always points from the perturber to the emitter). In addition, when coherently excited Auger states overlap in energy, either because of their natural widths, or the field of the target ion, interference effects can perturb the spectrum and angular distribution. Some of these effects, when significant, can have severe impact upon the extraction of unambiguous information about the collision process from the observed Auger spectrum.

The following discusses briefly those aspects of the PCI phenomena that could impact upon our measurements. Since the angular distributions of Auger intensities are determined in this work by referencing peak areas to the area of a nearby ^2S line, they are sensitive only to *differential* PCI effects between the two lines.

Recent observations of the focusing of Auger electrons (and diffraction) by the perturbing ion field have been reported by Swenson et al. [18], [19] and have been treated theoretically [19], [21]. These effects are prominent at small angles (a few degrees) in the forward (or backward) direction depending upon which particle is the emitter. We have made a classical calculation to estimate the importance of deflection of the Auger electron by the target product ion to our angular distribution measurements; a summary of this calculation is presented in the appendix. The effect is largest for backward emission from the lowest velocity projectile, and the state with the shortest Auger lifetime. In this work the largest effect is for the line from B^{2+} S_a produced by 20keV B^{4+} impact; at θ_{lab}=160° one obtains for the shift of the laboratory emission angle, $\Delta\theta_{lab}$=0.56° and an energy shift ΔE_T =–0.46 eV. The values of $\Delta\theta_{lab}$ produced by the post collision Coulomb scattering are not significant perturbations on the angular distributions measured in this work, and use of an asymetric gaussian function adequately reproduces the observed PCI perturbed line shapes for the spectra from B^{4+} collisions for the purpose of obtaining an accurate integration of the line intensities.

Post collisional Stark mixing effects on the anisotropy of Auger emission have been discussed by Stolterfoht et al. [22] and Miraglia and Macek [23], with particular reference to He states excited by Li^+ impact. The two level treatment in [22] produced the dimensionless parameter:

$$\kappa = \frac{\Gamma}{v}\left(\frac{2q\,|\,d_{12}\,|}{\Delta E_{12}}\right)^{1/2}, \qquad \text{(IV.1)}$$

as a measure of the effectiveness of Stark mixing during the decay of the Auger states; $\Gamma = (\Gamma_1\Gamma_2)^{1/2}$ with $\Gamma_{1,2}$ the decay widths of the two states in the absence of mixing, v is

the relative velocity of the partners, ΔE_{12} is the energy separation of the unperturbed states, q is the charge of the perturbing ion, and d_{12} is the dipole matrix element between the unperturbed states. For the case of P_b mixed with D for B^{2+} and C^{3+} in our studies, one has for both ions $\kappa \approx 0.038 \mid d_{12} \mid^{1/2}$ (d_{12} in atomic units). Ref. [22] suggests that values of $\kappa \approx 0.1$ or larger indicate significant perturbation to the Auger anisotropy. For our cases this would require $\mid d_{12} \mid \approx 7.5$ au; this is equivalent to a radiative rate of $\approx 8 \times 10^8$ sec^{-1} which is of the same magnitude as that calculated by Davis and Chung [4] for the P_b - S_a transition in B^{2+}. However, examination of our data (Figures 5,6) do not reveal large components odd in $\cos\theta$, which would signify strong Stark mixing; nevertheless, there are small contributions of such terms apparent in some of the cases with the best statistical precision. The data for the P_b state of C^{3+} produced by 50 keV (v=0.41 au) collisions (see Fig. 5) perhaps show this best. A slight enhancement in the forward direction is observed. Examination of the residuals from the fit of Eq. (III.2) to these data yields the plot shown in Figure 7. This statistically significant but small residual effect may be the result of Stark mixing, but may also be simply a technical artifact not entirely removed by the normalization scheme. Because of its small size we have chosen not to include terms odd in $\cos\theta$ in our fits to determine the anisotropy parameters; their inclusion would not significantly alter the values obtained. For the moment, we leave open the question of the origin of this small forward/backward asymmetry in the data.

V. L and M_L State Population Fractions

From the σ_L/σ_0 values extracted from the fits to the anisotropy data and the areas of the S_a and S_b peaks we have determined the variation with energy of the fractional population for the P_b, D, S_a and S_b states summed over all M_L quantum numbers. As discussed earlier these are the states produced directly in the double capture process. These results are presented in Figures 8 (a) and 9 (a) for the two ions, together with results from theoretical calculations by Fritsch and Lin [24] and by Hansen and Taulbjerg [25,26]. Note that we did not observe a significant presence of S_b in our boron measurements; this is consistent with the small fraction calculated in [24] and [26].

For the case of carbon we carried out additional measurements to determine the variation with energy of the total relative cross section for each state. That is, with all conditions held constant, we collected spectra using beams of varying energy at a single fixed angle in one continuous data collecting period. Using the previously measured anisotropy parameters we then extracted values proportional to the total cross section for each ^2L state. These data are presented in Figure 10. In principle this could have been extracted from the same data used to obtain the anisotropy parameters, however, those measurements were separated in time, and detector, gain and threshold values varied. Thus a separate series of measurements was made following the determination of the anisotropy parameters.

From the anisotropy parameters, A_{2k}, one may obtain the cross section ratios σ_{M_L}/σ_0 (see Ref. [2]). In the laboratory frame, with z-axis along the beam direction, one has, for a P state:

$$\frac{\sigma_1}{\sigma_0} = \frac{1-A_2/2}{1+A_2}, \tag{V.1}$$

and for a D state:

$$\frac{\sigma_1}{\sigma_0} = \frac{1+A_2/2-2A_4/3}{1+A_2+A_4}\ , \quad \frac{\sigma_2}{\sigma_0} = \frac{1-A_2+A_4/6}{1+A_2+A_4}. \tag{V.2}$$

Alternatively, one may extract a population fraction, f_{M_L}, for each substate $|L,M_L>$. Thus for a P state:

$$f_0 = \frac{1}{3}[1+A_2]\ , \ f_1 = \frac{1}{3}[1-A_2/2], \tag{V.3}$$

and for a D state:

$$f_0 = \frac{1}{5}[1+A_2+A_4]\ , \ f_1 = \frac{1}{5}[1+A_2/2-2A_4/3]\ , \ f_2 = \frac{1}{5}[1-A_2+A_4/6]. \tag{V.4}$$

In Figures 8 (b,c) and 9 (b,c) we present the $|LM_L>$ population fractions for the P_b and D states respectively together with the calculated values from Refs. [24], [25], and [26].

VI. Discussion

In a general sense, the extent to which the double capture population of the states studied in this work is understood is reflected in the degree of agreement between the calculations and the measurements evident in Figures 8, 9 and 10. The theoretical treatments [24, 25, 26] utilize close-coupling methods with limited two-electron basis sets, and treat the screening of the projectile nucleus by its 1s electron via model potentials. The work of Hansen and Taulbjerg [25,26] has stressed the imprtance of using a correlated set for the doubly excited states of the Li-like projectile state formed in the collision. When compared to calculations using a simpler basis set made up of products of hydrogenic

functions for the n=2 state, the superiority of the correlated basis was clearly evident. Of course, as pointed out in Ref. [25], it is well known that doubly excited states often show a high degree of correlation and thus it is not surprising that a limited basis set which includes the lowest order effects of the interelectronic repulsion performs better than one which treats the two electrons as independent particles moving in a screened central Coulomb potential. On the other hand, Fritsch and Lin [24] have obtained good agreement for the distribution of population among the L-states for B^{4+},He (see figure (8a)) using an atomic basis expansion in products of modified hydrogenic functions.

With regard to the M_L sublevel populations, generally there is good agreement between the calculations and the measurements for the higher velocities, but substantial deviation at low velocity for the D state formed in the B^{4+},He collision (Fig (8c)) and the P_b state formed in the C^{5+},He collision (Fig (9b)). In the latter case, Ref. [26] predicts a population distribution favoring M_L=1 near v=0.2 au; this is directly opposite the measured results.

In spite of the substantial theoretical progress, there is a strong desire to develop a physical picture or simple model which could explain, perhaps only qualitatively, the alignment observed in these, and future, multiple capture experiments. Toward this end one can use the measured anisotropy parameters to construct a picture of the charge cloud, averaged over all rotations about beam direction. An example of this is shown in Fig. 11 for the D states in the two systems studied. In molecular terminology, the initial state of the systems studied is Σ (M_L=0, laboratory frame ie, z-axis along the beam direction) and would remain such if only radial couplings were operative during the collision. This case is shown as the dashed shape at the bottom of Fig. 11,

and would be approached in the limit of zero collision velocity. The fact that Π and Δ states are formed (M_L=1,2) is caused by rotational coupling, which accounts for the inability of the electron motion to adiabatically follow the rotation of the internuclear axis during the transfer process. For the P_b states, one can parameterize the observed anisotropy in terms of an angle of "slippage", β, which is determined by assuming that all the population is formed in the M_L=0 sublevel in a frame with the internuclear axis making an angle β with respect to the beam direction. However this simple picture cannot reproduce the observed results for the D states, because a single β, at each velocity, will not reproduce the measured A_2 and A_4 values.

Recently the degree of orientation produced in single electron capture collisions has been addressed [27], in part, to see if the concept of a propensity rule favoring one orientation, as is applicable to excitation collisions, applies to the electron transfer process. Orientation, of course, cannot be determined by an experiment such as ours, since we do not define the collision plane. However some restrictions on the magnitude of the orientation and the relative phase of substate amplitudes can be extracted from the alignment measurements for the P_b state. Reflection symmetry requires that, in the collision frame (z-axis normal to the collision plane, x axis along the beam direction), only M_L=$\pm$1 substates are populated with complex amplitudes a_1 and a_{-1}. The orientation parameter (expectation value of L_z) $L_\perp$ is given by,

$$L_\perp = \frac{|a_1|^2 - |a_{-1}|^2}{|a_1|^2 + |a_{-1}|^2} \qquad \text{(VI.1)}$$

and the alignment angle, γ, which is the angle between the major axis of the ^2P_b charge cloud and the x-axis, is given by,

$$\gamma = \frac{1}{2}[\pi + \arg(a_{-1}a_1^*)]. \qquad \text{(VI.2)}$$

Since $a_0 \equiv 0$, $|a_1|^2 + |a_{-1}|^2 = 1$ and $L_\perp = 1 - 2|a_{-1}|^2$.

In the laboratory frame used in this work, with z axis along the beam direction (reached by rotation of the collision frame by $\pi/2$ about the y axis), γ and L_- determine the substate fractions, so that e.g.

$$f_0 = \frac{1}{2} + \frac{1}{2}F_0(v), \qquad \text{(VI.3)}$$

where F_0 is given by:

$$F_0(v) = \frac{2\pi}{\sigma_L}\int_0^\infty P_0(b,v)bdb(+)[1-L_\perp^2(b,v)]^{1/2}\cos[2\gamma(b,v)], \qquad \text{(VI.4)}$$

with P_0 (b,v) the probability density for populating the $M_L=0$ sublevel (laboratory frame) in a collision with relative velocity v and impact parameter b.

Note that our measured values of f_0 for all velocities in the B^{4+} collisions are near 1/2, and thus $F_0 \approx 0$. This would follow from $L_\perp^2$ (b,v) $\approx$ 1, or $\gamma(b,v) \approx \pi/4$ (or $3\pi/4$) for all significant impact parameters, or wide variation of $2\gamma(b,v)$ with impact parameter so that rapid oscillation of $\cos(2\gamma)$ causes the integral to be near zero. Thus one can at most say that the observations for B^{4+} are consistent with large values for $L_\perp(b,v)$ over the significant impact parameter range, but do not require this to be true. The C^{5+} measurements of f_0 for the P_b state, differ substantially from 1/2, especially at the higher velocities (i.e. $f_0=0.24$ at v=0.50 au). This suggests that in the region of impact parameters contributing to population of $M_L=0$, $L_\perp^2(b,v)$ deviates significantly from unity and $\gamma(b,v)$ lies in the range $\pm\pi/4$ about $\gamma=\pi/2$ for these collisions. Clearly, definitive answers to questions regarding the orientation of the charge cloud in a double capture collision await further experimental progress aided and accompanied by

advanced calculations.

Anisotropy can substantially affect inferences drawn from Auger intensity measurements made at a single angle. It is common to find measurements made at a laboratory angle of zero degrees, where there is minimal kinematic broadening, or 50 degrees to gain the high efficiency of a cylindrical mirror spectrometer mounted coaxial with the beam (see e.g. Ref. [28]). The quantity $\Delta_L(\theta) \equiv W_L(\theta) - 1$ is the deviation of the intensity observed at θ, in the emitter frame, from that which would be emitted by an isotropic source of the same total intensity. For Auger decay from a P state to a final S state, such as from the P_b level in this work, observation at 50° in the laboratory, together with the kinematic shift at velocities near 0.5 au make the emitter frame angle very near the "magic" angle $\theta = \cos^{-1}(1/3)^{1/2}$ where $P_2(\cos\theta)=0$, so the intensity observed can be used as a direct measure of the cross-section for producing the P state. This is not the case for D to S transitions. There is no general "magic" angle for this case and Δ_D can be substantial at both 50° and 0°. Fig. 12 shows the variation with velocity of Δ_D at these two angles for the C^{5+},He system obtained from the measured A_2 and A_4 parameters. The point at zero velocity follows from the fact that, in this somewhat artificial case, all population must be in the $M_L=0$ sublevel. A smooth curve has been fit between the zero velocity points and the measured points between v=0.2 and 0.5 au. The portion of the curve between v=0 and v=0.2 is dashed to indicate that nature may follow a different path. Note that at v=0.5 au, measurements made at 50° exceed the equivalent isotropic intensity by 30 percent, while those made at zero degrees fall short by about 50 percent. Assuming the dashed curve represents reality, observations at 50° at v=0.1 would underestimate the total intensity by about 60%. This type of error can

propagate in treatments where fractional intensities, observed at a single angle, in lines from different L states, is equated to fractional populations for the excited states. Since the normalizing intensity is the sum of that from all lines, including those with perhaps substantial Δ_L values, even S states (or P states observed at the magic angle) can be misrepresented. The degree of error, of course, must be evaluated for each case.

Such an analysis was carried out by Posthumus, Lukey and Morgenstern [29] in their study of the population of 3l3l′ states formed by double capture from He and H_2 targets based upon the assumption that in the collision frame, only the M_L=+L sublevel was populated. Predicted populations of states within the 3l3l′ configuration based on this assumption and a modified version of the classical overbarrier model which includes angular momentum effects, were in good agreement with their observations of Auger intensities at 50° in the laboratory when bare projectiles C^{6+} and O^{8+} were used. Agreement was not good for the two-electron projectiles N^{5+}, and O^{6+} in collision with H_2. Our observations of anisotropy are inconsistent with the assumption that, e.g., the D state is formed entirely in the M_L=+2 sublevel in the collision frame over the velocity range studied for the B^{4+},He and C^{5+},He systems. If this were the case one would not observe strong velocity variation of the substate populations; these would be fixed at f_0=3/8, f_1=1/4 and f_2=1/16 for any projectile. Our results for the B^{4+},He system (Fig. (8c))are close to these values near v=0.5 au, while the results for the C^{5+},He system (Fig. (9c)) approach them near v=0.2, but deviate strongly as the velocity increases. If one assumes that only M_L=2 and M_L=0 are populated in the collision frame (population of M_L=±1 are forbidden by reflection symmetry), then one can easily show that in the laboratory frame one should have $f_1 \leq 1/4$. This is satisfied by the results obtained with

B^{4+} projectiles but not by those with the C^{5+} ions. The B^{4+} D-state results are consistent with collision frame populations in M_L=2 ranging from 0.88 at v=0.47 au down to 0.50 at v=0.25 with the remaining population in M_L=0. One can also calculate a mean phase angle $[\arg(a_2^* a_0)]$ between the M_L=2 and M_L=0 amplitudes to be near 90 degrees in this model. The C^{5+} results require that some population be present in each of the M_L=2,0,-2 sublevels in the collision frame.

Recently Lundsgaard and Lin [30] have demonstrated the utility of a propensity rule favoring population of the M_L=−L sublevel (in the collision frame) in calculating the result of single electron capture by C^{6+} from H atoms. Of course, for experiments such as ours (or those of Posthumus et al. [29]), which do not fix the collision plane, there is no difference between assuming that all population is in the M_L=+L or −L sublevels. Either choice predicts the same outcome when transformed to the laboratory frame (z-axis along the projectile beam); an outcome which is only partially consistent with our measurements of the D state sublevel population fractions as discussed above.

The question remains then, as to the validity of the assumption of Posthumus et al. (and the propensity rule discussed in [30]). Perhaps it is most appropriate only for pure one-, or two-electron collision systems; this would be consistent with their and our observations that it is considerably less useful for He-like and H-like projectiles colliding with H_2 and He respectively at velocities in the range of 0.2-0.5 au.

Acknowledgment

We gratefully thank C. Lyneis of the LBL Nuclear Science Division for valuable assistance. This work was performed under the auspices of the U.S. Department of Energy by Lawrence Livermore National Laboratory under Contract No. W-7405-Eng-48, and by Lawrence Berkeley Laboratory with support from the Director, Office of Energy Research, Office of Basic Energy Sciences, Chemical Sciences Division, U.S. Department of Energy under Contract No. DE-AC03-76SF00098.

Appendix: Classical Deflection of the Auger Electron Trajectory

For electron emission from the projectile at a distance r from the target product ion of charge Q_T, at rest at the coordinate origin, the laboratory energy of the electron is shifted from its unperturbed value, E_{lab}, by an amount $\Delta E_T = -(Q_T/r)$ and the shift, $\Delta\theta_{lab}$, of the electron trajectory in the laboratory from its unperturbed emission angle θ_{lab} is:

$$\Delta\theta_{lab} = \cos^{-1}\left[\frac{\alpha}{(\alpha^2+1)^{1/2}}\right] \pm \cos^{-1}\left[\frac{\rho+\alpha}{(\alpha^2+1)^{1/2}}\right] - \theta_{lab} \,, \tag{A.1}$$

where the +(−) sign is taken for $\theta_{lab} \geq \pi/2$ ($\theta_{lab} \leq \pi/2$),

$$\alpha = -\frac{\Delta E_T}{2\sin\theta_{lab}} \frac{1}{(E_{lab}E')^{1/2}} \,, \tag{A.2}$$

$$\rho = (E_{lab}/E')^{1/2}\sin\theta_{lab} \,, \tag{A.3}$$

and

$$E' = E_{lab} + \Delta E_T \, . \tag{A.4}$$

$E_{lab}=E_{em}+\Delta E_K(\theta_{lab})$ is kinematically shifted from the emitter frame Auger line energy, E_{em}, by the amount:

$$\Delta E_K = E_c(2\cos\theta_{lab}[(E_{em}/E_c)-\sin^2\theta_{lab}]^{1/2} - 2\sin^2\theta_{lab} + 1) \, , \tag{A.5}$$

where $E_c=(m_e/M_P)E_P$, is the laboratory energy of an electron at rest in the projectile rest frame (E_P, and M_P are the projectile energy and mass, m_e the electron mass).

This treatment for $\Delta\theta_{lab}$ is valid provided r is much larger than the collision impact parameter, taking $r=v\tau$, with v the projectile velocity, and τ the excited state lifetime, one has values ranging from r=100-200 au for the lines studied here, whereas the important impact parameters are near a few au. Integrating the energy shift, ΔE_T, over all separations weighted by the emission rate $(v\tau)^{-1}e^{-r/v\tau}dr$, one obtains the Barker-Berry [20] asymmetric line shape with full width at half maximum, $1.07\Delta E_T$, and peak intensity at E′.

Table 1. B^{2+} 1s2l2l′ state properties. $A_{R,A}$=total radiative, Auger decay rates, τ=lifetime, ΔE=natural width, δE=fine structure shift from the level of lowest J, E_A=Auger electron energy. Numbers in brackets indicate the power of 10 by which the entry is to be multiplied.

State	J	A_R (sec^{-1})	A_A (sec^{-1})	τ (sec)	ΔE (meV)	δE (meV)	E_A (eV)
$1s2s^2\ ^2S$	1/2			1.06[-14][h]	62.2[h]	0.0	154.84[h]
$1s2s2p\ ^4P$	1/2	2.05[5][c]	1.44[8][c]	6.94[-9][c]	9.48[-5][c]	0.0	156.64[c]
	3/2	4.87[5][c]	5.48[7][c]	1.81[-8][c]	3.64[-5][c]	-0.78[b]	"
	5/2	≈0.0*	3.37[6][c]	2.97[-7][c]	2.22[-6][c]	4.31[b]	"
$1s[2s2p\ ^3P]^2P$	1/2	2.78[11][a]	6.15[12][a]	1.56[-13][a]	4.2[a]	0.0	161.02[c]
	3/2	"	"		"	5.00[b]	"
$1s2p^2\ ^4P$	1/2	4.54[8][d]	3.20[6][d]	2.19[-9][d]	3.01[-4][d]	0.0	163.93[d]
	3/2	"	2.07[7][d]	2.10[-9][d]	3.13[-4][d]	3.84[g]	"
	5/2	"	2.33[8][d]	1.45[-9][d]	4.54[-4][d]	4.92[g]	"
$1s[2s2p\ ^1P]^2P$	1/2	3.24[10][a]	4.65[13][a]	2.15[-14][a]	30.6[a]	0.0	163.89[c]
	3/2	"	"	"	"	-1.40[b]	"
$1s2p^2\ ^2D$	3/2	1.28[11][a]	6.39[13][a]	1.56[-14][a]	42.2[a]	0.0	166.15[c]
	5/2	"	"	"	"	-6.87[b]	"
$1s[2p^2\ ^3P]^2P$	1/2	4.3[11][f]				0.0	167.08[f]
	3/2	"				4.2[f]	"
$1s2p^2\ ^2S$	1/2	1.23[11][a]	1.03[13][a]	9.59[-14][a]	6.9[a]	0.0	170.96[d]

*This level may decay by magnetic quadrupole radiation to $1s^22s$, but the rate is insignificant for low Z ions.

a=Ref. [4], b=Ref. [5], c=Ref. [6], d=Ref. [7], e=Ref. [8], f=Ref. [9], g=Ref. [10], h=Ref. [11]

Table 2. C^{3+} 1s2l2l′ state properties. $A_{R,A}$=total radiative, Auger decay rates, τ=lifetime, ΔE=natural width, δE=fine structure shift from the level of lowest J, E_A=Auger electron energy. Numbers in brackets indicate the power of 10 by which the entry is to be multiplied.

State	J	A_{rad} (sec^{-1})	A_{Auger} (sec^{-1})	τ (sec)	ΔE (meV)	δE (meV)	E_{Auger} (eV)
$1s2s^2\ ^2S$	1/2	2.91[10]^e	7.48[13]^e	1.34[-13]^e	49.1^e	0.0	226.8^a
$1s2s2p\ ^4P$	1/2	1.57[6]^b	3.31[8]^b	3.01[-9]^b	2.2[-4]^b	0.0	229.3^b
	3/2	3.83[6]^b	1.06[8]^b	9.11[-9]^b	7.2[-5]^b	0.5^f	"
	5/2	≈0.0*	8.77[6]^b	1.14[-7]^b	5.8[-6]^b	12.2^f	"
$1s[2s2p\ ^3P]^2P$	1/2	6.88[11]^d	6.37[12]^d	1.42[-13]^d	4.6^d	0.0	235.2^b
	3/2	"	"	"	"	12.4^d	"
$1s2p^2\ ^4P$	1/2	5.89[8]^c	2.40[6]^c	1.69[-9]^c	3.9[-4]^c	0.0	238.5^c
	3/2	5.92[8]^c	1.94[7]^c	1.64[-9]^c	4.0[-4]^c	9.4^f	"
	5/2	5.93[8]^c	9.18[8]^c	6.62[-10]^c	9.9[-4]^c	14.4^f	"
$1s[2s2p\ ^1P]^2P$	1/2	6.86[10]^d	5.53[13]^b	1.81[-14]^b	36.4^b	0.0	238.7^b
	3/2	"	"	"	"	-1.3^d	"
$1s2p^2\ ^2D$	3/2	3.57[11]^d	7.97[13]^d	1.25[-14]^d	52.7^d	0.0	241.8^c
	5/2	"	"	"	"	13.7^d	"
$1s2p^2\ ^2P$	1/2	8.66[11]^e	4.91[8]^e	1.15[-12]^e	0.57^e	0.0	242.9^e
	3/2	"	9.80[9]^e	1.14[-12]^e	0.58^e	17.9^e	"
$1s2p^2\ ^2S$	1/2	2.55[11]^e	1.82[13]^e	5.42[-14]^e	12.1^e	0.0	247.9^c

*This level may decay by magnetic quadrupole radiation to $1s^22s$ but the rate is insignificant in low Z ions.

a=Ref. [12], b=Ref. [6], c=Ref. [7], d=Ref. [13], e=Ref. [14], f=Ref. [15]

Table 3. σ_L/σ_S, anisotropy coefficients, A_{2k}, and M_L substate fractions, f_{M_L}. Quantities in parenthesis are the experimental uncertainties in the last digit quoted (one standard deviation).

Ion(State)	v(au)	σ_L/σ_S	A_2	A_4	f_0	f_1	f_2
C^{3+}(D)	0.50	3.66(11)	0.32(6)	-0.82(9)	0.101(17)	0.342(31)	0.108(17)
	0.41	2.98(2)	0.33(1)	-0.67(2)	0.132(3)	0.322(5)	0.112(5)
	0.36	2.40(6)	0.35(5)	-0.40(7)	0.191(14)	0.288(17)	0.117(15)
	0.29	1.31(4)	0.60(8)	0.19(12)	0.357(27)	0.235(20)	0.087(18)
	0.22	0.61(3)	0.48(12)	0.30(15)	0.354(34)	0.208(25)	0.115(25)
$C^{3+}(P_b)$	0.50	7.90(25)	-0.28(5)		0.241(16)	0.380(8)	
	0.41	5.08(8)	-0.20(3)		0.267(9)	0.367(4)	
	0.36	3.19(9)	-0.17(5)		0.277(17)	0.361(8)	
	0.29	1.09(5)	0.12(10)		0.373(32)	0.313(16)	
	0.22	0.31(2)	0.27(17)		0.423(57)	0.288(29)	
B^{2+}(D)	0.47	0.649(15)	0.402(46)	0.154(69)	0.311(14)	0.220(12)	0.125(11)
	0.38	0.399(9)	0.451(48)	0.292(68)	0.349(15)	0.206(11)	0.120(11)
	0.33	0.354(15)	0.170(92)	0.48(12)	0.329(27)	0.153(21)	0.182(21)
	0.25	0.326(16)	-0.185(95)	0.43(13)	0.249(26)	0.124(25)	0.251(26)
$B^{2+}(P_b)$	0.47	0.899(18)	0.481(40)		0.494(13)	0.253(7)	
	0.38	0.642(15)	0.651(51)		0.550(17)	0.225(9)	
	0.33	0.444(17)	0.576(84)		0.525(28)	0.237(14)	
	0.25	0.266(7)	0.389(63)		0.463(21)	0.269(10)	

References

*Work performed while on leave at Lawrence Livermore National Laboratory, and Lawrence Berkeley Laboratory.

**Work performed while on leave from Wesleyan University at Lawrence Livermore National Laboratory, and Lawrence Berkeley Laboratory.

[1]R. Hoekstra, F.J. de Heer and R. Morgenstern, Z. Phys D **21**, S81 (1991).

[2]W. Melhorn, in *Atomic Inner-Shell Processes* edited by B. Crasemann (Plenum Press, New York 1985) pp 119,180.

[3]R.A. Holt, M.H. Prior, K.L. Randall, R. Hutton, J. McDonald and D. Schneider, Phys. Rev. **A43**, 607 (1991); MS thesis, K.L. Randall, Wesleyan Univ., LLNL report #UCRL-ID-106591 (1990).

[4]B.F. Davis and K.T, Chung, Phs. Rev. A **31**, 3017 (1985).

[5]K.T. Chung and R. Bruch, Phys. Rev. A **28**, 1418 (1983).

[6]B.F. Davis and K.T. Chung, Phys. Rev. A **39**, 3942 (1989).

[7]B.F. Davis and K.T. Chung, Phys. Rev. A **37**, 111 (1988).

[8]K.T. Chung, R. Bruch, E. Träbert and P.H. Heckmann, Physica Scripta **29**, 108 (1984).

[9]R. Bruch, K.T. Chung, E. Träbert, P.H. Heckmann, B. Raith, and H.R. Mueller, J. Phys. B: At. Mol. Phys. **17**, 333 (1984).

[10]J. Hata and I.P. Grant, J. Phys. B: At. Mol. Phys. **16**, 915 (1983).

[11]B.F. Davis and K.T. Chung, Phys. Rev. A, **29**, 1878 (1984).

[12]R. Bruch, K.T. Chung, W.L. Luken, and J.C. Culberson, Phys. Rev. A **31**, 310 (1985).

[13]B.F. Davis and K.T. Chung, private communication.

[14]M.H. Chen, Atomic Data and Nuc. Data Tables, **34**, 301 (1986).

[15]K.T. Chung, Phys. Rev. A **29**, 682 (1984).

[16]W. Melhorn and K. Taulbjerg, J. Phys. B **13**, 445 (1980).

[18]J.K. Swenson, C.C. Havener, N. Stolterfoht, K. Sommer and F.W. Meyer, Phys. Rev. Letters **63**, 35 (1989).

[19]J.K. Swenson, J. Burgdörfer, F.W. Meyer, C.C. Havener, D.C. Gregory, and N. Stolterfoht, Phys. Rev. Letters, **66**, 417 (1991).

[20]R.O. Barrachina, and J.H. Macek, J. Phys. B **22**, 2151 (1989).

[21]R.B. Barker and H.W. Berry, Phys. Rev. **151**, 14 (1966).

[22]N. Stolterfoht, D. Brandt and M. Prost, Phys. Rev. Letters **43**, 1654 (1979).

[23]J.E. Miraglia and J. Macek, Phys. Rev. **A42**, 3971 (1990).

[24]W. Fritsch and C.D. Lin, Phys. Rev. **A45**, 6411 (1992).

[25]J.P. Hansen and K. Taulbjerg, Phys. Rev. **A45**, R4214 (1992).

[26]J.P. Hansen and K. Taulbjerg, Phys. Rev. **A47**, 2987 (1993).

[27]J.P. Hansen, L. Kocbach, A. Dubois, and S.E. Nielsen, Phys. Rev. Letters **64**, 2491 (1990).

[28]See for example M. Mack, Nuc. Instruments and Methods in Phys. Res. **23**, 74 (1987).

[29]J.H. Posthumus, P. Lukey and R. Morgenstern, J. Phys. B: At. Mol. Opt. Phys. **25**, 987 (1992).

[30]M.F.V. Lundsgaard and C.D. Lin, J. Phys. B: At. Mol. Opt. Phys. **25**, L429 (1992).

Figure Captions

Figure 1. Plan view of the joint LBL/LLNL atomic physics facilities and the ECR ion source located at the LBL 88-inch Cyclotron.

Figure 2. Sketch of the rotatable parallel plate electron spectrometer and gas jet target assembly used in this work.

Figure 3. The Auger spectrum obtained at a laboratory angle of 160° showing lines from the decay of B^{2+} 1s2l2l′ levels formed by double electron capture from He by B^{4+} ions at a collision energy of 40 keV. The energy scale and the intensities have been transformed to the emitter frame. The lines are asymmetric gaussian curves fit to the data.

Figure 4. Auger lines from the decay of C^{3+} 1s2l2l′ levels populated by double capture from He atoms by 50keV C^{5+} ions. The laboratory angle was 160°, and the energy scale and intensities have been transformed to the emitter frame. The lines are gaussian curves fit to the data.

Figure 5. Anisotropy in the intensity of Auger emission from the P_b level of (a) B^{2+}, and (b) C^{3+}, resulting from double electron capture by B^{4+} and C^{5+} ions from He at four, and five collision velocities, respectively. The curves are fits to the data of the function $W(\theta)$, (see Eq. (III.2)). The fits yield the anisotropy parameter A_2 at each velocity.

Figure 6. Anisotropy in the intensity of Auger emission from the D level of (a) B^{2+},

and (b) C^{3+}, resulting from double electron capture by B^{4+} and C^{5+} ions from He at four and five collision velocities, respectively. The curves are fits to the data of the function $W(\theta)$, Eq. (III.2); the fits yield the anisotropy parameters, A_2 and A_4.

Figure 7. Residuals from the fit of $W(\theta)$ to the C^{3+} P_b anisotropy data at 50 keV (v=0.41 au) collision energy. A small forward/backward asymmetry is evident; see text for discussion.

Figure 8. Results for the B^{4+},He system. (a) shows the L-state population fractions; (b) and (c) show the P_b and and D state magnetic sublevel fractions, f_{M_L}, versus collision velocity. The long dashed lines are results of calculations by Fritsch and Lin [24], and the short dashed lines are those by Hansen and Taulbjerg [26].

Figure 9. Results for the C^{5+},He system. (a) shows the L-state population fractions; (b) and (c) show the P_b and and D state magnetic sublevel fractions, f_{M_L}, versus collision velocity. The dashed lines are results of calculations by Hansen and Taulbjerg, [26] in (a),(b), and [25] in (c).

Figure 10. Velocity variation of the total cross section for producing all ^{2}L levels of the C^{3+} 1s2l2l′ configuration and the partial cross sections for each ^{2}L level by double capture of C^{5+} ions from He atoms.

Figure 11. Comparison of the charge cloud shapes, rotationally averaged about the beam direction (arrow), for the $1s2p^2$ ^{2}D states of B^{2+} (left) and C^{3+} (right) formed by double capture from He atoms by B^{4+} and C^{5+}. The dashed shape at the bottom is that

expected in the limit of zero velocity collisions where only Σ states may be populated.

Figure 12. Velocity variation of the deviation, Δ_D, of the C^{3+} D state Auger intensity observed at 0° and 50° laboratory viewing angles from that expected for equally populated sublevels (isotropic emitter). The points at zero velocity follow from the condition that only M_L=0 (laboratory frame) would be populated in this limit. The other points are from the measurements.

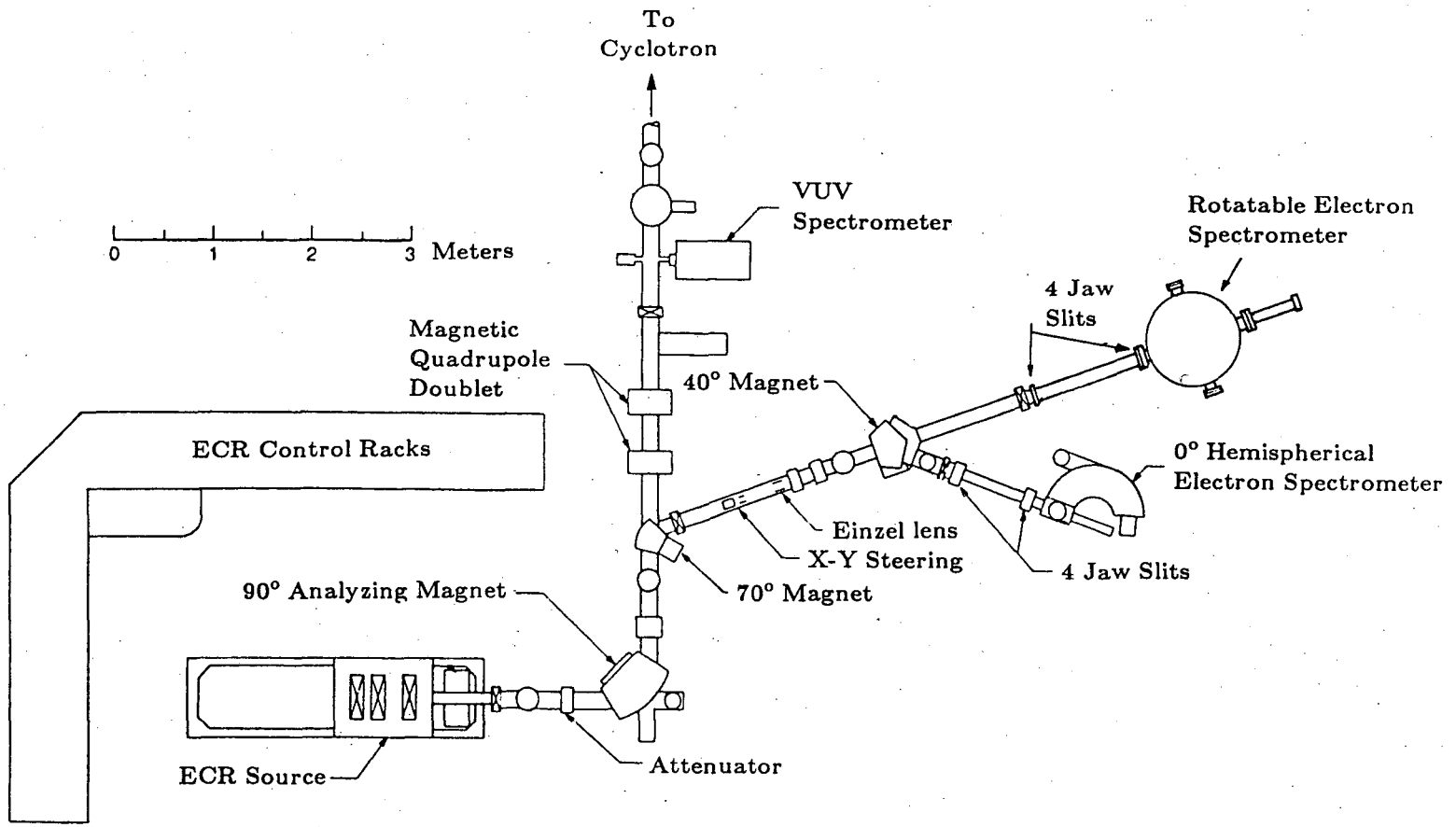
To
Cyclotron
VUV
Spectrometer
Rotatable Electron
Spectrometer
0 1 2 3 Meters
4 Jaw
Slits
Magnetic
Quadrupole
Doublet
40° Magnet
ECR Control Racks
0° Hemispherical
Electron Spectrometer
Einzel lens
X-Y Steering
4 Jaw Slits
90° Analyzing Magnet
70° Magnet
ECR Source
Attenuator

XBL 908-2811

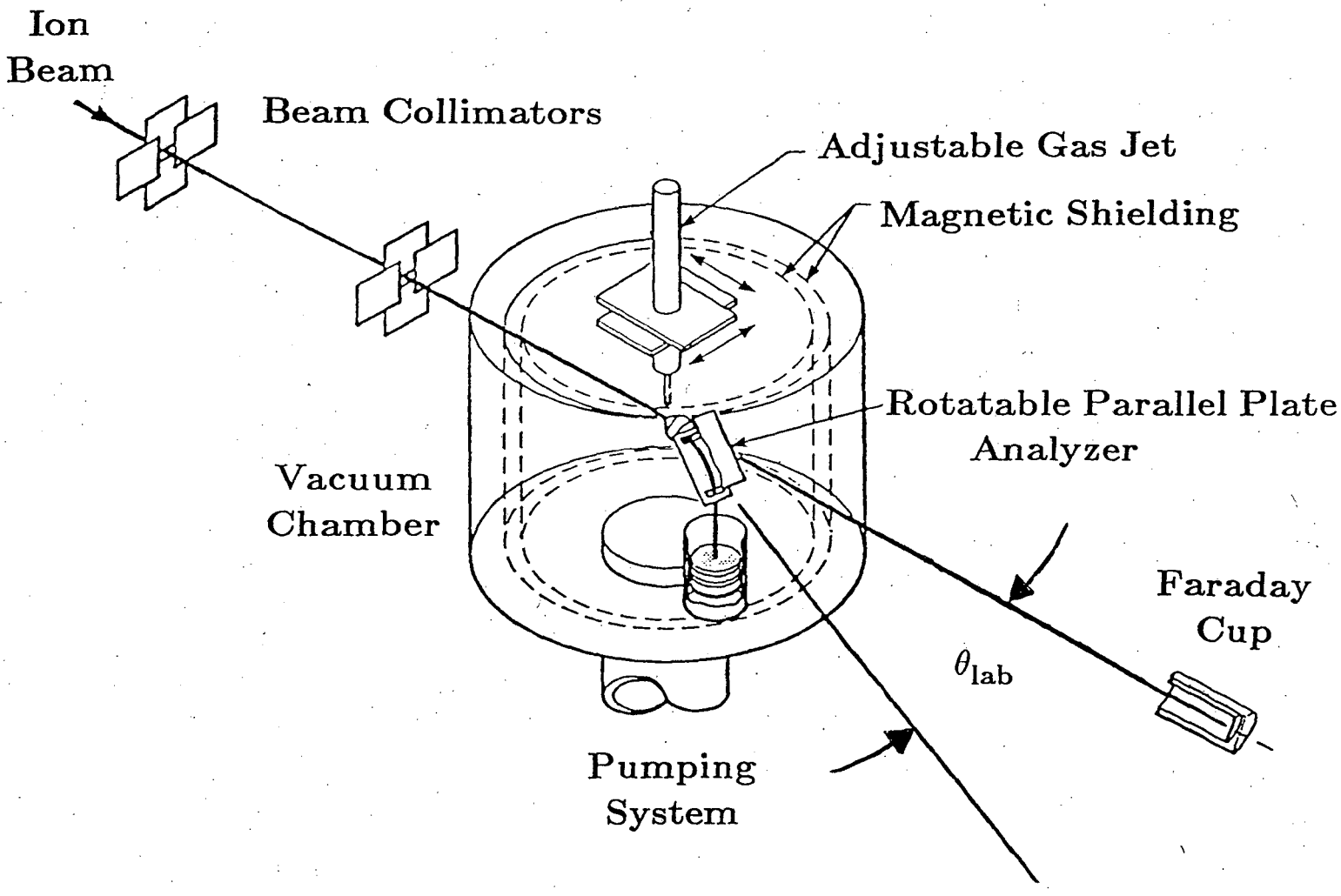
Ion
Beam
Beam Collimators
Adjustable Gas Jet
Magnetic Shielding
Rotatable Parallel Plate
Analyzer
Vacuum
Chamber
Faraday
Cup
θ_{lab}
Pumping
System

Fig.2

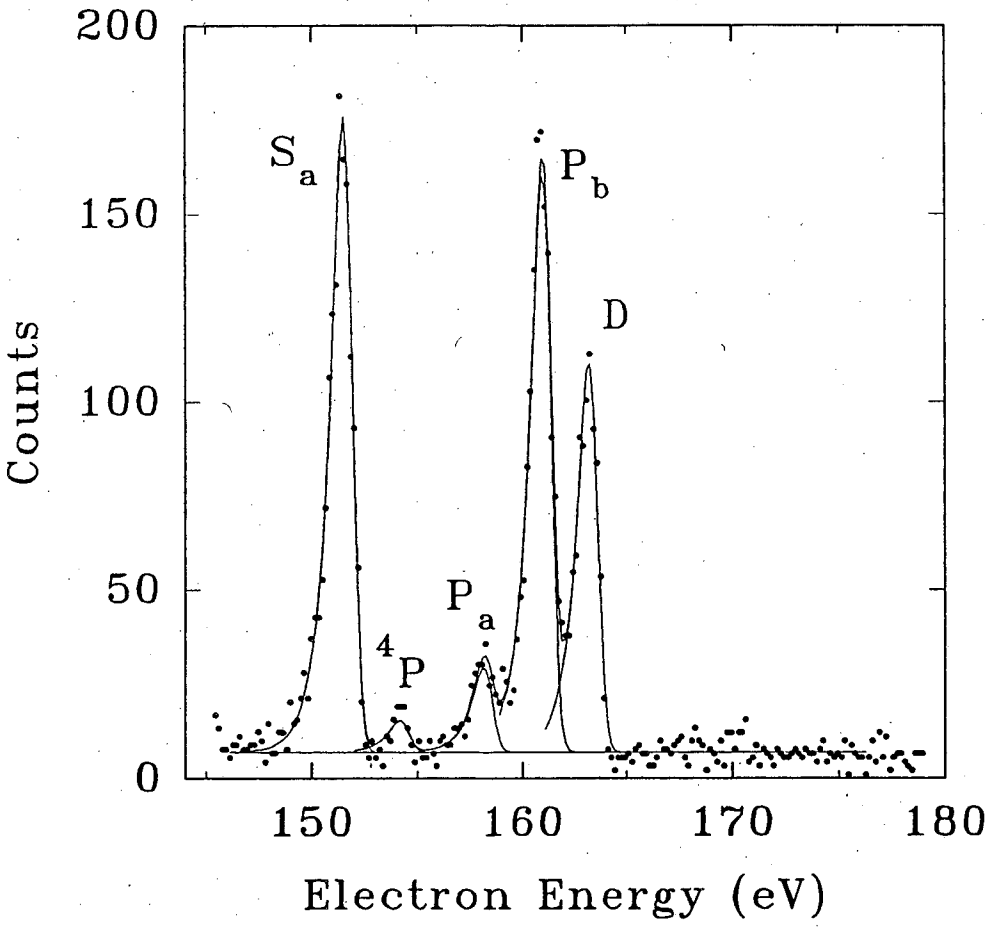
200
150
100
50
0
Counts
S_a
P_b
D
P_a
^4P
150
160
170
180
Electron Energy (eV)

Fig. 3

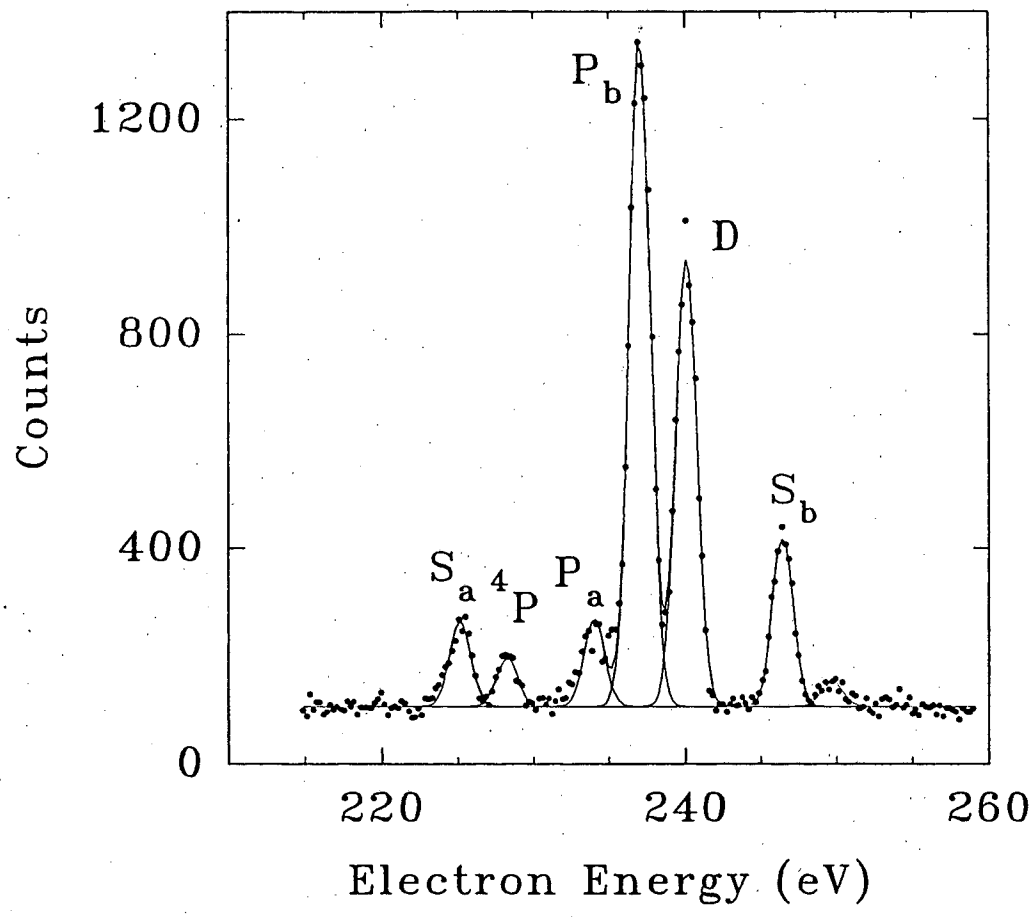
1200
800
400
0
Counts
220
240
260
Electron Energy (eV)
P_b
D
S_b
S_a
^4P
P_a

Fig. 4

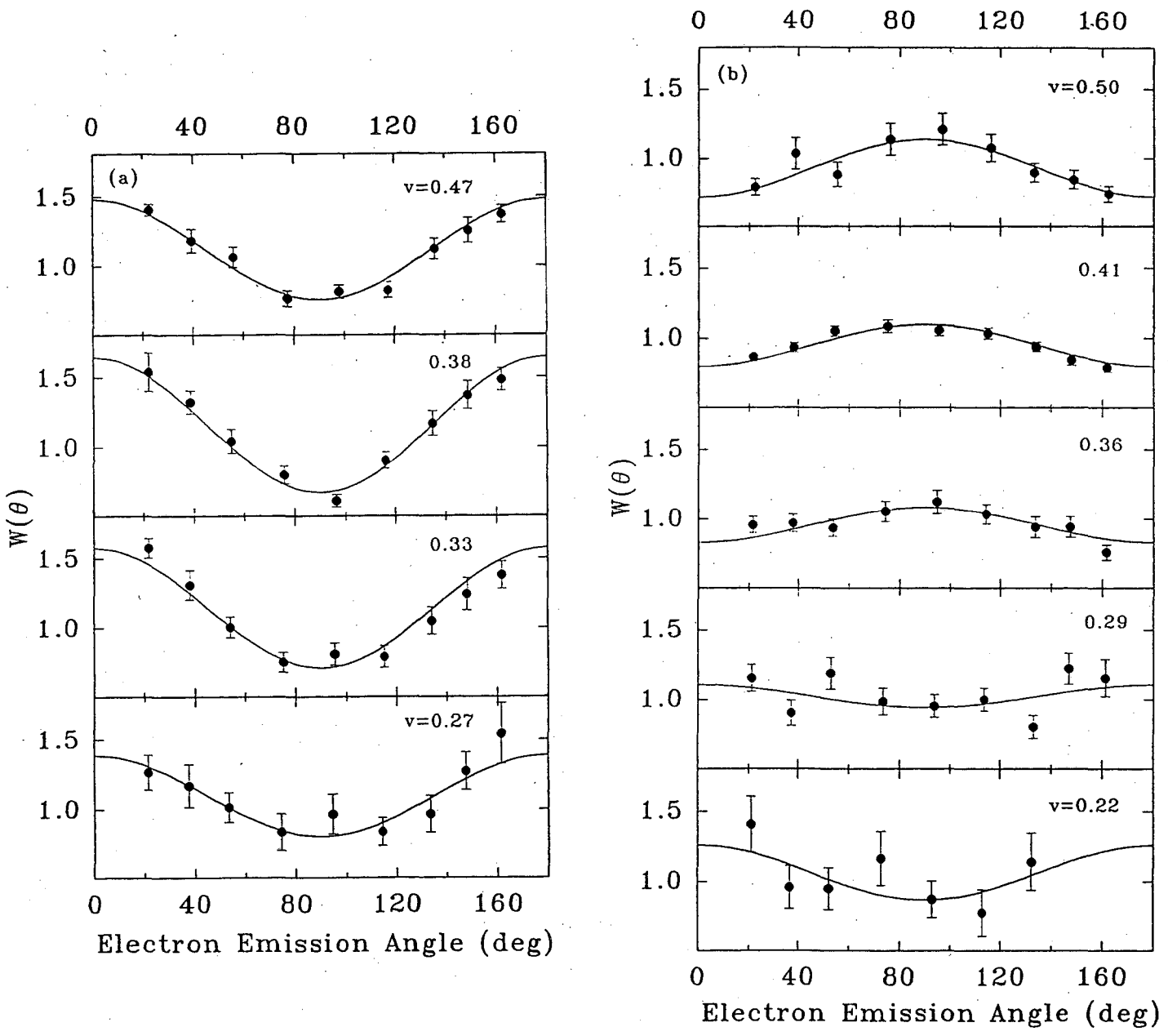
(a)
v=0.47
0.38
0.33
v=0.27
(b)
v=0.50
0.41
0.36
0.29
v=0.22
W(θ)
0
40
80
120
160
1.0
1.5
Electron Emission Angle (deg)

Fig. 5

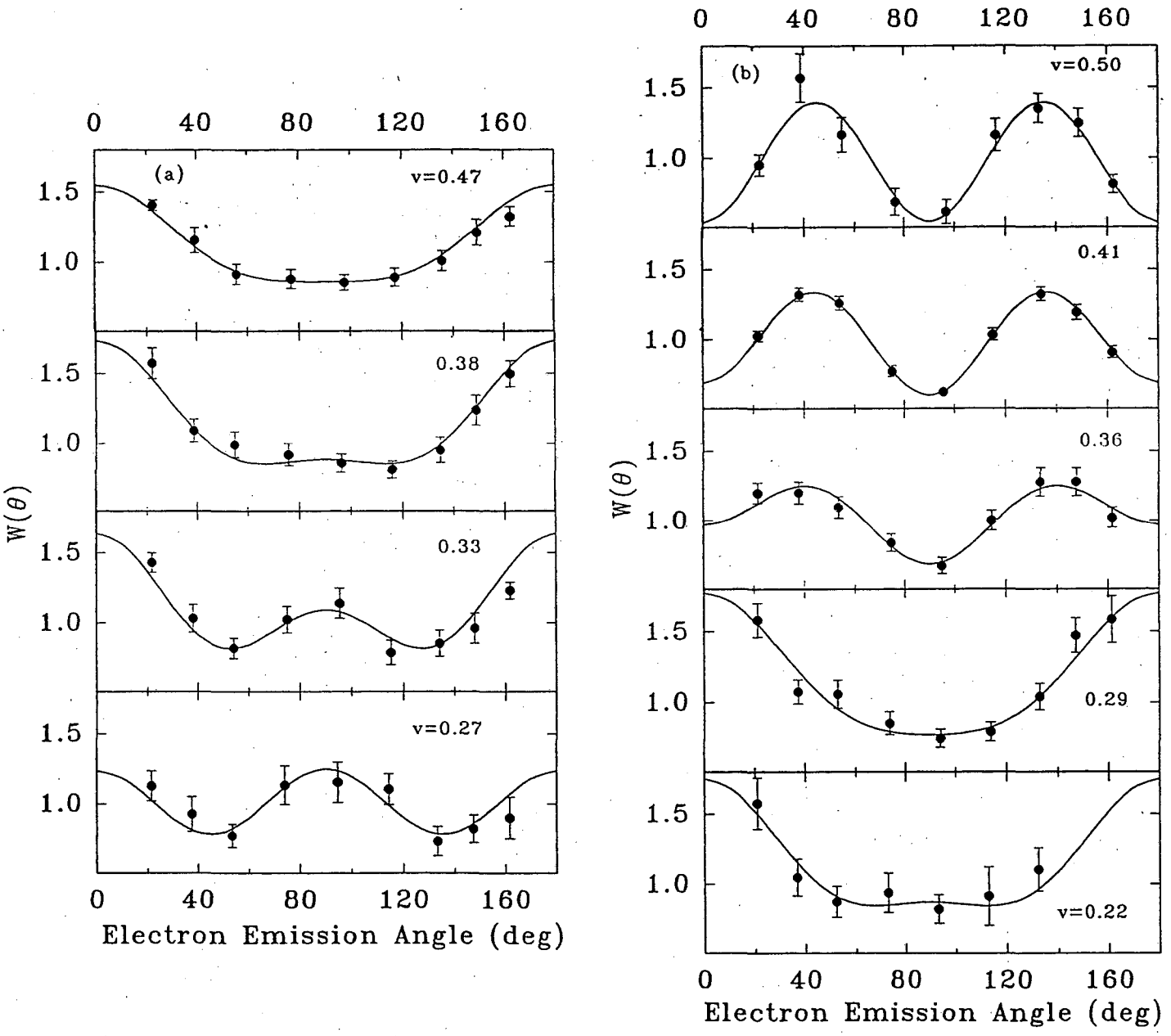
(a)
v=0.47
0.38
0.33
v=0.27
(b)
v=0.50
0.41
0.36
0.29
v=0.22
W(θ)
Electron Emission Angle (deg)

Fig. 6

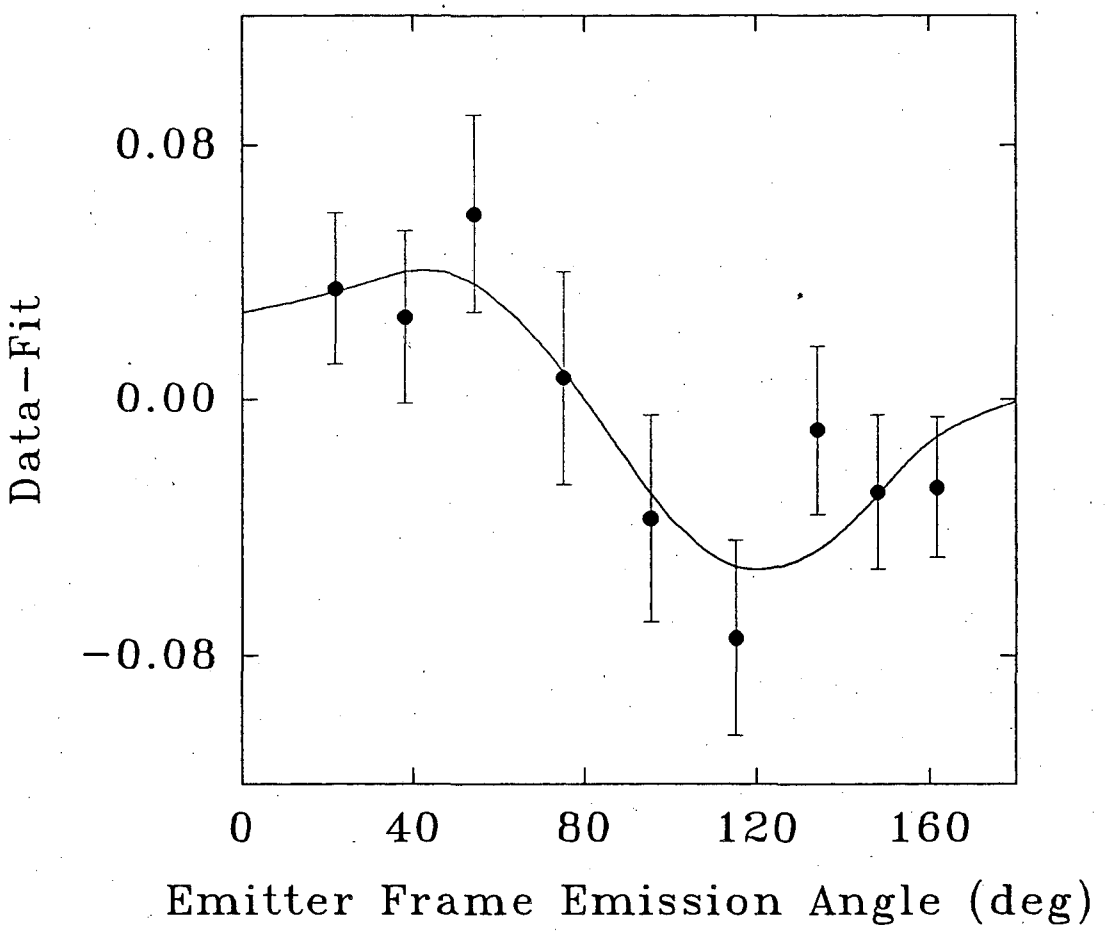
0.08
0.00
−0.08
Data−Fit
0
40
80
120
160
Emitter Frame Emission Angle (deg)

Fig. 7

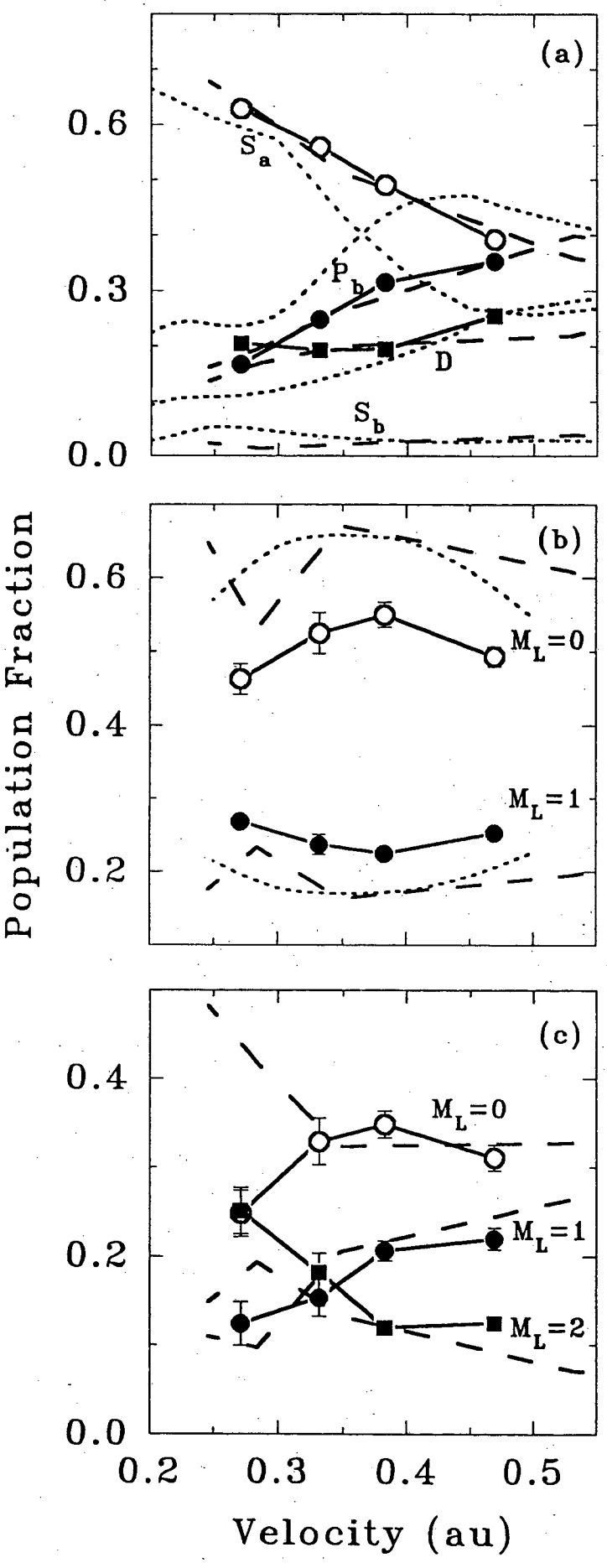
(a)
0.6
0.3
0.0
S_a
P_b
D
S_b
(b)
0.6
0.4
0.2
$M_L=0$
$M_L=1$
Population Fraction
(c)
0.4
0.2
0.0
$M_L=0$
$M_L=1$
$M_L=2$
0.2
0.3
0.4
0.5
Velocity (au)

Fig. 8

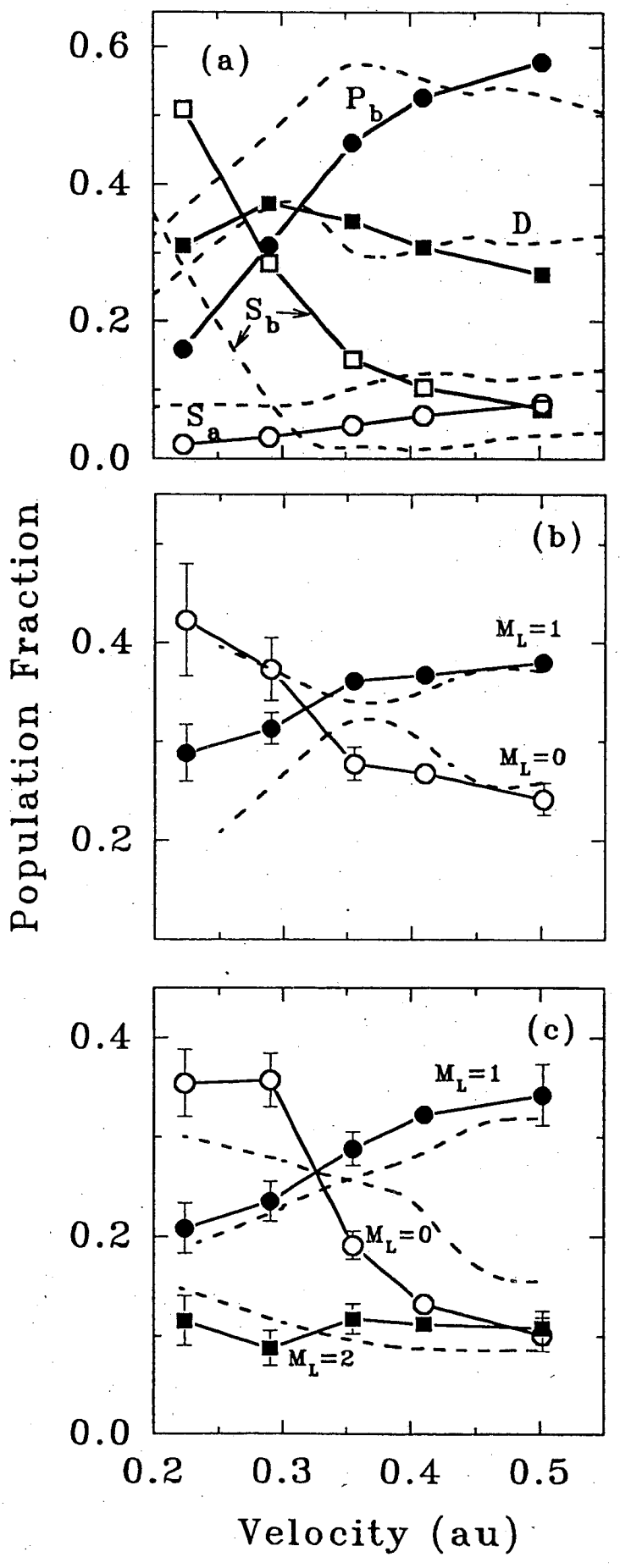
(a)
P_b
D
S_b
S_a
(b)
$M_L=1$
$M_L=0$
(c)
$M_L=1$
$M_L=0$
$M_L=2$
Population Fraction
Velocity (au)
0.0
0.2
0.4
0.6
0.2
0.3
0.4
0.5

Fig. 9

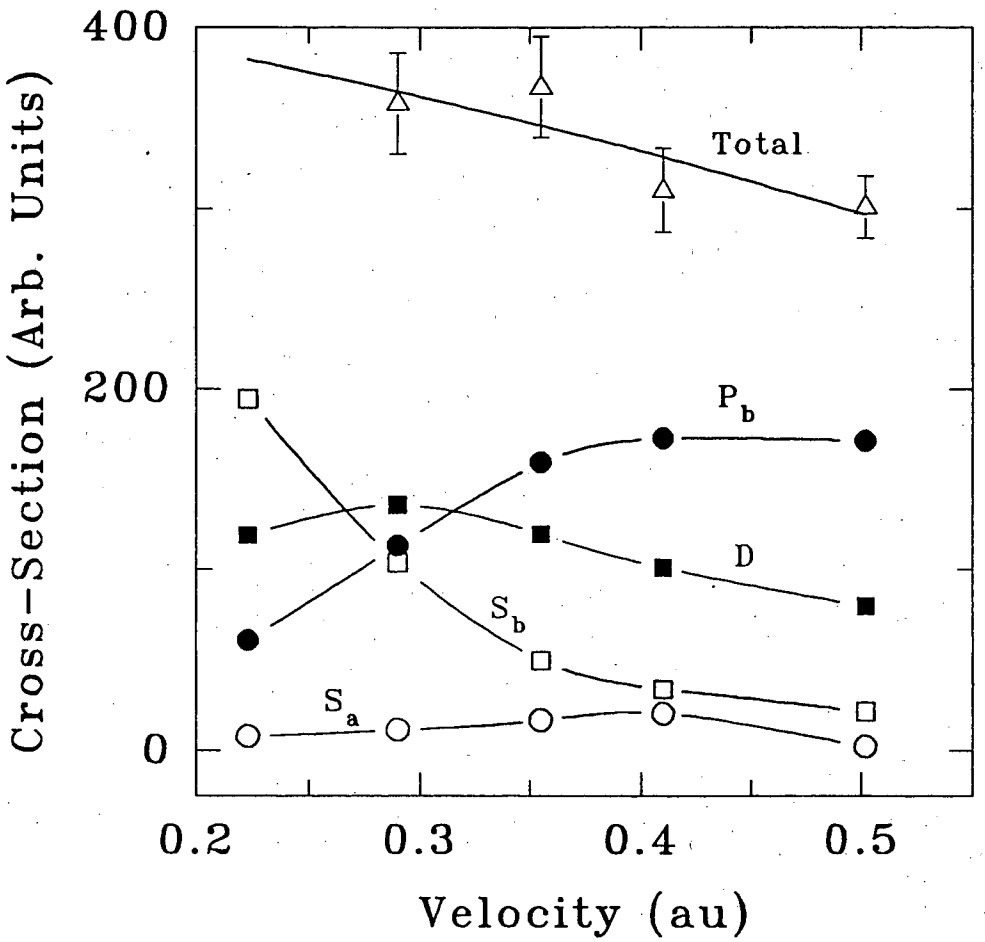
400
200
0
Cross-Section (Arb. Units)
Total
P_b
D
S_b
S_a
0.2
0.3
0.4
0.5
Velocity (au)

Fig. 10

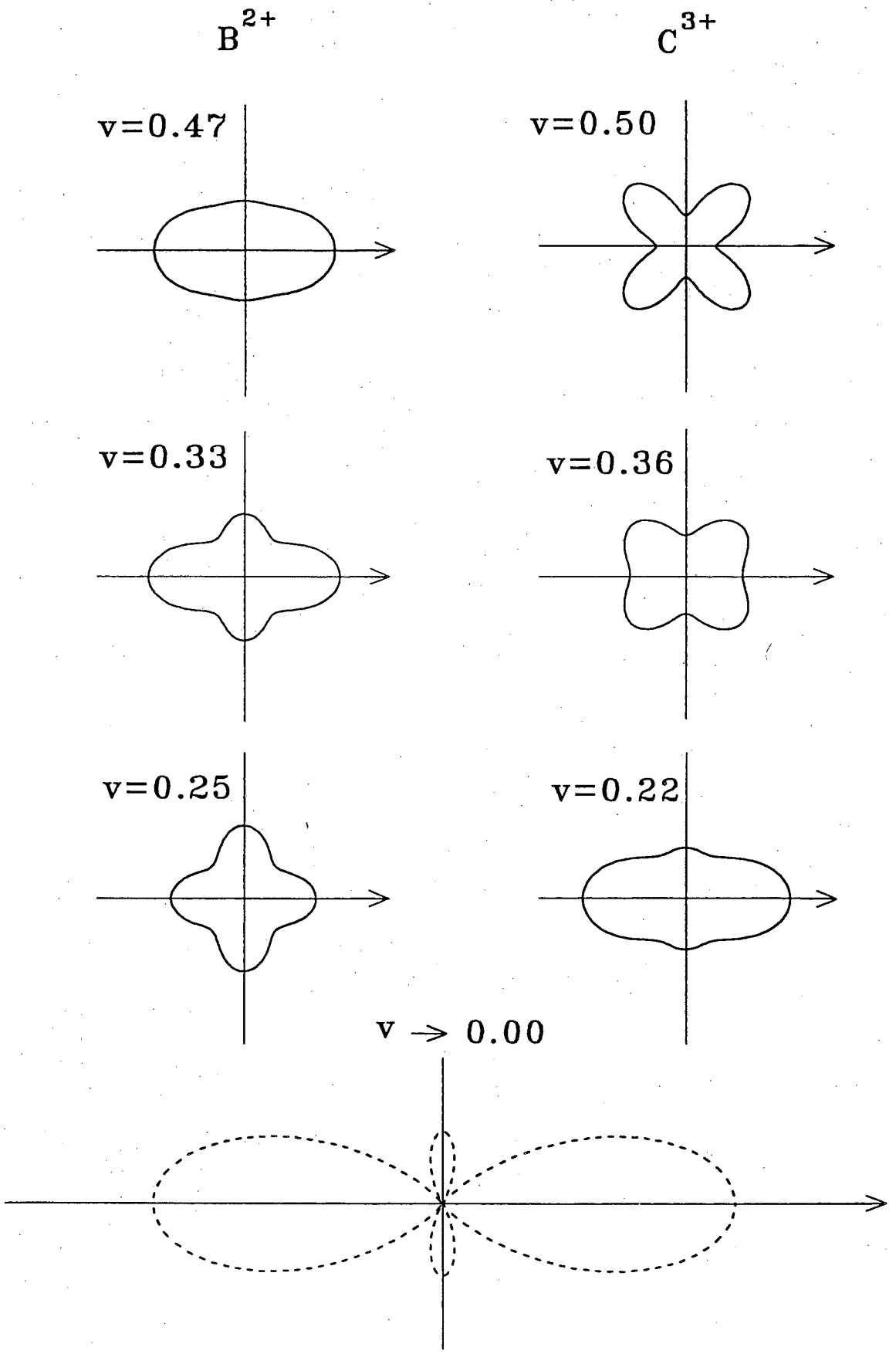

Fig. 11

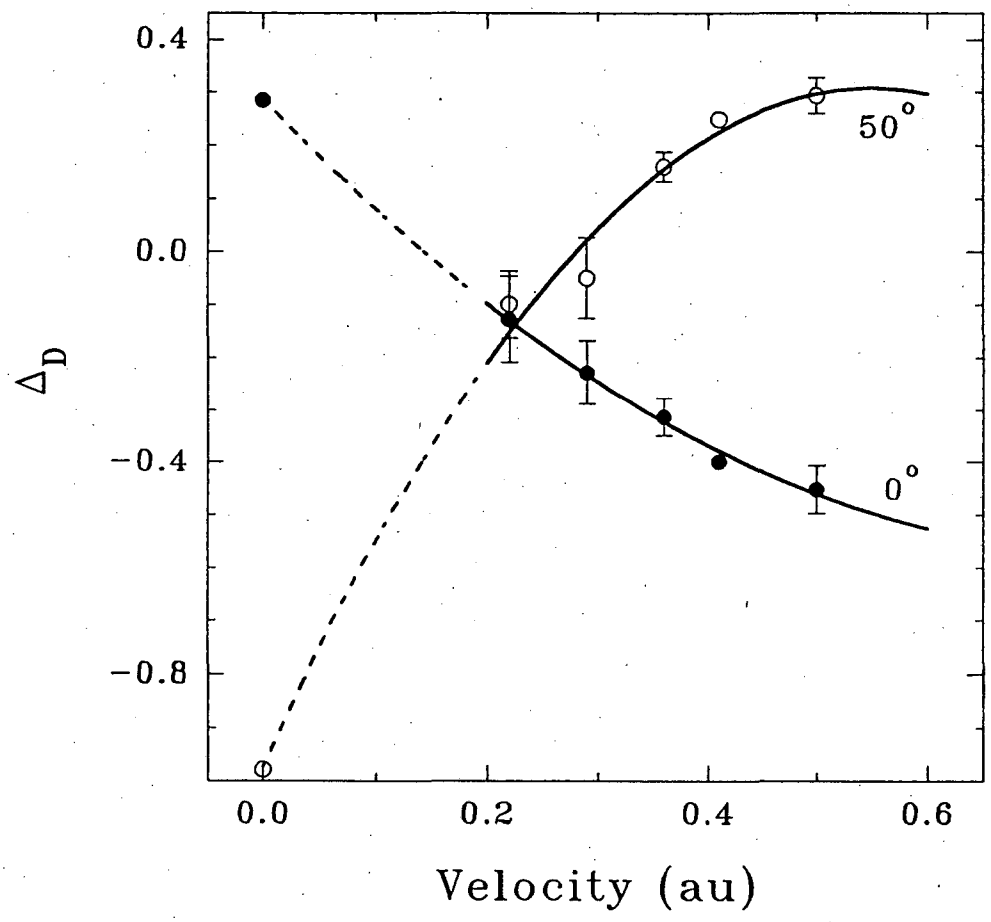

Fig. 12

LAWRENCE BERKELEY LABORATORY
UNIVERSITY OF CALIFORNIA
TECHNICAL INFORMATION DEPARTMENT
BERKELEY, CALIFORNIA 94720